



**HAL**  
open science

# Comparison between multi-frequency and multi-speed laser lock-in thermography methods for the evaluation of crack depths in metal

Christine Boué, Stéphane Holé

► **To cite this version:**

Christine Boué, Stéphane Holé. Comparison between multi-frequency and multi-speed laser lock-in thermography methods for the evaluation of crack depths in metal. Quantitative InfraRed Thermography Journal, 2020, 17 (4), pp.223-234. 10.1080/17686733.2019.1635351 . hal-04017948

**HAL Id: hal-04017948**

**<https://hal.sorbonne-universite.fr/hal-04017948v1>**

Submitted on 7 Mar 2023

**HAL** is a multi-disciplinary open access archive for the deposit and dissemination of scientific research documents, whether they are published or not. The documents may come from teaching and research institutions in France or abroad, or from public or private research centers.

L'archive ouverte pluridisciplinaire **HAL**, est destinée au dépôt et à la diffusion de documents scientifiques de niveau recherche, publiés ou non, émanant des établissements d'enseignement et de recherche français ou étrangers, des laboratoires publics ou privés.

**Comparison between multi-frequency and multi-speed laser lock-in thermography methods for the evaluation of crack depths in metal**

C. Boué, S. Holé

*Sorbonne Université, F-75005 Paris, France*

LPEM, CNRS, ESPCI Paris, PSL Université Paris, 10 rue Vauquelin, F-75005 Paris, France

christine.boue@espci.fr

# **Comparison between multi-frequency and multi-speed laser lock-in thermography methods for the evaluation of crack depths in metal**

Two original methods using lock-in thermography with a laser excitation are proposed for the estimation without contact of open crack depths in metal. The first uses a modulated punctual thermal source and is well suited for the study of complicated structures. In the second, a continuous moving thermal source allows to scan homogeneous structures. Each method relies on the heat diffusion modifications induced by a crack located in the thermal diffusion area of the synchronised heat source. The thermal signature of the crack is extracted to the amplitude of surface temperature images for various modulation frequencies or various scanning speeds of the thermal source. The thermal signatures are analysed according to a length representative of the thermal diffusion length to give a local evaluation of the crack depth. The obtained results demonstrate the potentiality of active lock-in thermography as a contactless measurement tool for the evaluation of crack depths up to 3 mm.

Keywords: Infrared thermography, lock-in thermography, non-destructive testing, crack depth, crack sizing, laser heating

## **1. Introduction**

Metallic systems that are submitted to mechanical stresses can develop cracks which can trigger large damages detrimental to safety. Consequently, crack depth is an essential information to appreciate its possible dangerousness. The active infrared (IR) thermography is a non-contact and non-destructive technique widely used for the inspection of components, especially for perpendicular crack detection [1-4]. In this technique, the structure under study is excited by a heat source and the disturbances of the heat diffusion are analyzed. However, the discontinuity of the heat diffusion which reveals a crack depends also on parameters like the surface state of the sample, the

crack width and the spatial configuration of the heating excitation [5-9]. Consequently, the evaluation of the crack depth is difficult to extract.

In [10,11], two original methods using lock-in thermography are presented to directly evaluate open crack depths without requiring any calibration procedure. The crack has to be located inside the thermal diffusion area of a heating source. Used as a 3D probe of the crack depth, the thermal diffusion length is adjusted by the modulation frequency of a punctual heat source [10] or by the speed of a moving continuous heat spot [11]. The evolution of the first or second order spatial derivatives of the amplitude and of the phase images obtained in synchronism with the heating source for different frequencies or speeds is representative of the crack depth. However, these operators are sensitive to large emissivity gradients, especially at the edges of the crack where the information is used in calculation.

In this work, it is chosen to analyse the thermal response of an area back of the crack, in its “shadow”, in order to obtain a more robust method. 3D Finite Element Method (FEM) numerical results from COMSOL Multiphysics are used to introduce new indicators for each method. These new developments to improve sensitivity and accuracy of the measurements are presented and analyzed.

## **2. Stimulated lock-in thermography methods**

A crack located in the thermal diffusion area of a thermal source acts as a thermal barrier which modifies locally the heat diffusion. The main instrumental difference between the two methods presented for the crack depth evaluation is the heating process which is “multi-frequency” or “multi-speed”. Thereafter, the heating process is in synchronism with the acquisition process of an IR camera.

## 2.1 Multi-frequency laser stimulated lock-in thermography

A modulated laser spot excitation heats the sample surface at different frequencies  $f$  in order to heat more or less deeply the sample (Figure 1a). The different frequencies of the modulated heating source have to be correctly chosen, according to the thermal diffusivity  $D$  of the studied material. The thermal diffusion length is:

$$\mu = \sqrt{\frac{D}{\pi f}} \quad (1)$$

This length is used as a 3D scan parameter for the sample. Using a lock-in thermography detection, the unwanted continuous (DC) heating component is filtered out from the raw images of the IR camera. The surface temperature variation is calculated for each pixel by fast Fourier transform (FFT) in synchronism with the modulated heat source for each frequencies.

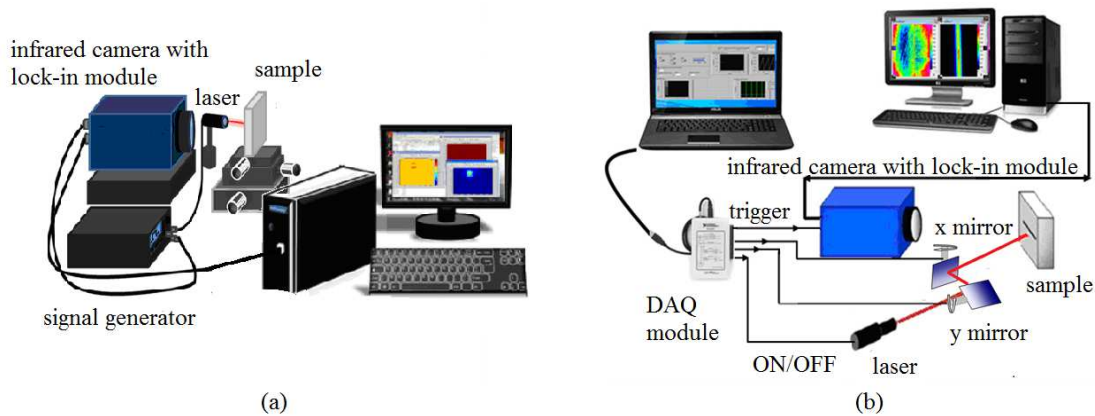


Figure 1. Experimental set-ups (a) multi-frequency lock-in thermography (b) multi-speed lock-in thermography

## 2.2 Multi-speed continuous laser stimulated lock-in thermography

A continuous heating laser spot moves aside the crack at different speeds  $v$  in order to heat more or less deeply the sample (Figure 1b). The different speeds for the displacement  $L$  of the heating source have to be correctly chosen, depending on the

thermal diffusivity of the studied material. In that case, the thermal diffusion length used as a 3D scan parameter for the sample is:

$$\mu = \sqrt{\frac{DL}{\pi\nu}} \quad (2)$$

The surface temperature variation at frequency  $\nu/L$  is calculated for each pixel by fast Fourier transform (FFT) in synchronism with the heat source displacement for each speeds.

### 3. Improved procedure for the crack depth evaluation

Previously [10,11], the crack depth signatures were extracted from the first or the second spatial derivative of the amplitude and phase images for the studied parameters (frequencies or speeds according to the chosen method). However, the reflected and emitted IR radiations vary brightly in the presence of sharp surface edges. Consequently, the spatial derivatives are directly impacted by the crack edges in real measurements, inducing uncertainties in the crack depth estimation.

In the improved procedure, the crack signature is extracted from the amplitude image  $A_{sh}$  of a shadow area located back of the crack (not on the crack), in the crack area where the heat diffusion can modify the surface temperature of the sample after bypassing the crack (Figure 2a). The crack depth signature is normalized by the amplitude  $A_0$  obtained at low frequency (low speed) in the reference area in symmetry with the heating spot where the amplitudes correspond to those expected in case of absence of crack (Figure 2b).

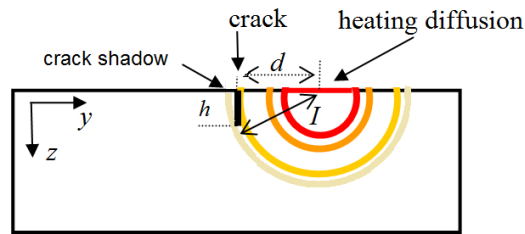
For FEM simulations, tetrahedral meshing is adapted to the various domains of the sample (bulk or vicinity of the crack). The number of mesh elements is about 6000 in the air block, and about 170000 in the metallic block. A surface mesh example is shown in Figure 2c. At the top of the surface, a finer mesh is used close to the crack in

order to be able to calculate temperature variations with a sufficient spatial resolution.

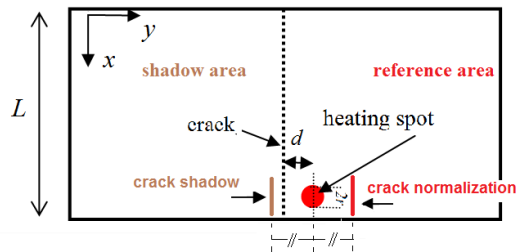
In this model, the influence of radiative and convective heat transfer is neglected.

Across the lateral sides, the insulated boundary condition is assumed. The thermal diffusivity  $D$  is  $3.3 \text{ mm}^2/\text{s}$  which corresponds to Inconel alloy thermal diffusivity and the open crack width is  $40 \text{ }\mu\text{m}$ . Figure 3a shows the amplitude image obtained with a punctual heat source ( $f = 0.1 \text{ Hz}$ ) on a simulated uniform crack of  $1 \text{ mm}$  depth.

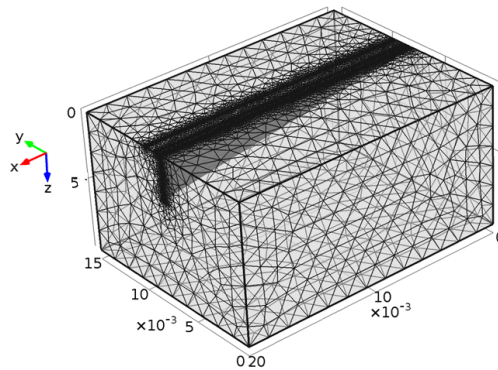
Figure 3b represents the amplitude image of a simulated varying  $0\text{-}3\text{-mm}$  crack depth using a moving continuous heat spot ( $v=L/\Delta t$  with  $\Delta t = 5 \text{ s}$  and  $L = 30 \text{ mm}$ ). The linear crack footprint is clearly visible at the left of the heat sources for both images.



(a)



(b)



(c)

Figure 2. Sample model (a) in depth (y,z directions) (b) in surface (x,y directions). The crack shadow is located at the left of the crack and the reference area is located at the right of the heating spot.  $d$  is the distance of the heat source to the crack,  $h$  is the crack depth and  $r$  is the radius of the heat source. (c) Typical surface mesh in (x,y,z) directions used for FEM simulations in case of a non constant crack depth.

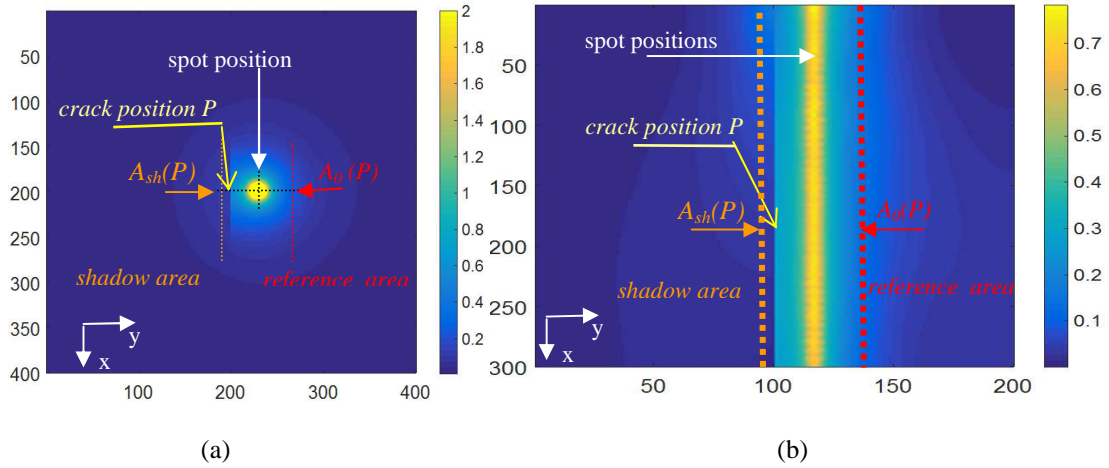


Figure 3. Simulated amplitude images  $A$  (arbitrary units a.u.), with a distance of the heat source to the crack  $d = 1.25$  mm and a radius of the heat source  $r = 0.25$  mm. (a) case of punctual heat source, modulation frequency  $f = 0.1$  Hz, simulated crack depth  $h(x) = 1$  mm, 1 pixel represents  $70 \mu\text{m} \times 70 \mu\text{m}$ . (b) case of moving continuous heat source, displacement over 30mm during  $\Delta t = 5$  s ( $v/L=0.2$  Hz). 1 pixel represents  $100 \mu\text{m} \times 100 \mu\text{m}$ . Simulated crack depth  $h(x)=x/100$  ( $x$  in pixel,  $h$  in mm), depth  $h$  range: 0-3 mm.

A set of pixels  $P=\{x,y\}$  located on the crack which faces the heating zone are extracted from the spatial derivative of the image with a basic numerical processing described in [12]. The crack shadow pixels are chosen at a distance  $\Delta y$  of a few pixel from  $P$  in the shadow area. The amplitude of each crack shadow pixel is affected to the corresponding crack pixel  $P$ :  $A_{sh}(x,y)=A(x,y-\Delta y)$  for each frequency (speed) values.  $A_0(P)$  is obtained at low frequency (low speed) in symmetry with the heat spot in the reference area:  $A_0(x,y)=A(x,y+\Delta y+2*d)$ .  $A_{sh}(P)$  depends on the crack geometry, the

heating area and the frequency (the speed) of the heating spot while  $A_0(P)$  doesn't depend on the crack.

Figure 4 gives  $A_{sh}$  along the crack selected pixels (x direction) for 5 durations  $\Delta t$  between 0.5 s to 5 s. The resulting ratios  $A_{sh}/A_0$  and their second order polynomial fits  $f_h$  are presented in Figure 5 as a function of the normalized thermal diffusion length  $\mu/\mu_{max}$  where  $\mu_{max}$  is the maximum value of the chosen thermal diffusion lengths  $\mu$ , that is to say the thermal diffusion length at the lowest frequency (speed). The frequency (speed) set depends on thermal characteristics of the sample and on the experimental set-up (heating source power and lock-in sensitivity).

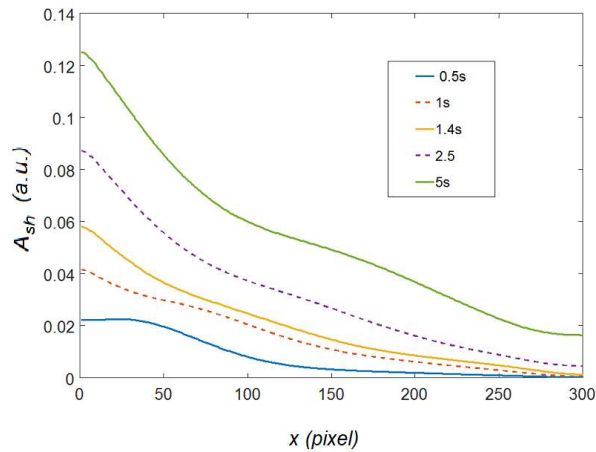


Figure 4.  $A_{sh}$  (arbitrary units) extracted from simulated amplitude images obtained for 5 displacement speeds along the 300 selected crack pixels. The simulated h depth is:  $h(x) = x/100$  where x is in pixel (1 pixel represents  $100\mu\text{m}$ ). Distance of the heat source to the crack is  $d = 1.25\text{mm}$ . Crack shadow pixels:  $\Delta y = 4$  pixels.

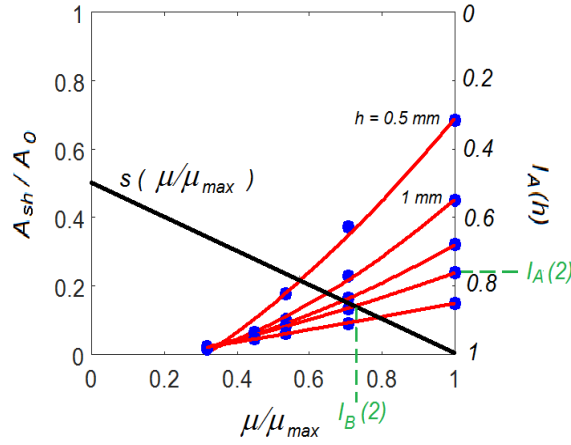


Figure 5.  $A_{sh}/A_0$  FEM results (blue dots) and their fits (red curves) as a function of  $\mu/\mu_{max}$  for 5 simulated depth values  $h$  (0.5 mm, 1 mm, 1.5 mm, 2 mm, 2.5 mm). The intersection of the  $A_{sh}/A_0$  curve and a linear function  $s$  (black line) gives the  $I_B$  indicator of the crack depth. The value  $1-(A_{sh}/A_0)_{max}$  at  $\mu/\mu_{max} = 1$  gives the  $I_A$  indicator of the crack depth. Simulated parameters: thermal diffusion length at the lowest frequency (speed)  $\mu_{max} = 2.3$  mm; Crack shadow pixels:  $\Delta y = 4$  pixels.

Two values are extracted from a  $A_{sh}/A_0$  fit curve to differentiate the crack depths. The first value is obtained for  $\mu/\mu_{max} = 1$ . The second one is chosen from the intersection between a linear decreasing function  $s(\mu/\mu_{max})$  and the fit curves.  $s(1) = 0$  allows to have a good sensitivity for high  $h$  value and  $s(0)$  is an adjustable sensitivity parameter for the differentiation of the  $h$  values. Though  $s(0)$  is not a very sensitive parameter. It is generally chosen equal to 0.5 for sake of simplicity. The value of  $A_{sh}/A_0$  for  $\mu/\mu_{max} = 1$  and the value of  $\mu/\mu_{max}$  at the intersection of  $A_{sh}/A_0$  with  $s$  are two local crack depth indicators  $I_A$  and  $I_B$ .  $I_A$  is defined as  $I_A = 1 - (A_{sh}/A_0)_{max}$  and  $I_B$  corresponds to the value  $\mu/\mu_{max}$  when  $f_h = s$ .

#### 4. Global crack depth indicator

The presented simulated results are calculated from a varying form to 0-3 mm crack depth using a moving continuous heat spot. Figure 6 presents  $I_A$  and  $I_B$  indicators for the 2 directions of the laser displacement (Figure 6a for increasing x and Figure 6b for decreasing x). It can be seen that the  $I_A$  have a better sensitivity for the low crack depths. When the crack depth increases,  $(A_{sh}/A_0)_{max}$  decreases so that  $I_A$  is affected by the thermal noise in case of real measurements. The global indicator  $I = I_A * I_B$  allows to improve the robustness of the evaluation especially for the practical measurements.

In these simulations, the scanning distance  $d$  between the laser and the crack is constant ( $d = 1.25 \text{ mm}$ ). The differences between the indicator responses with respect to the direction of the moving spot is due to heat accumulation of the moving heating spot. The direction of the heating source displacement introduces thus a bias so that it is chosen to average the responses  $I$  of the two scanned directions.

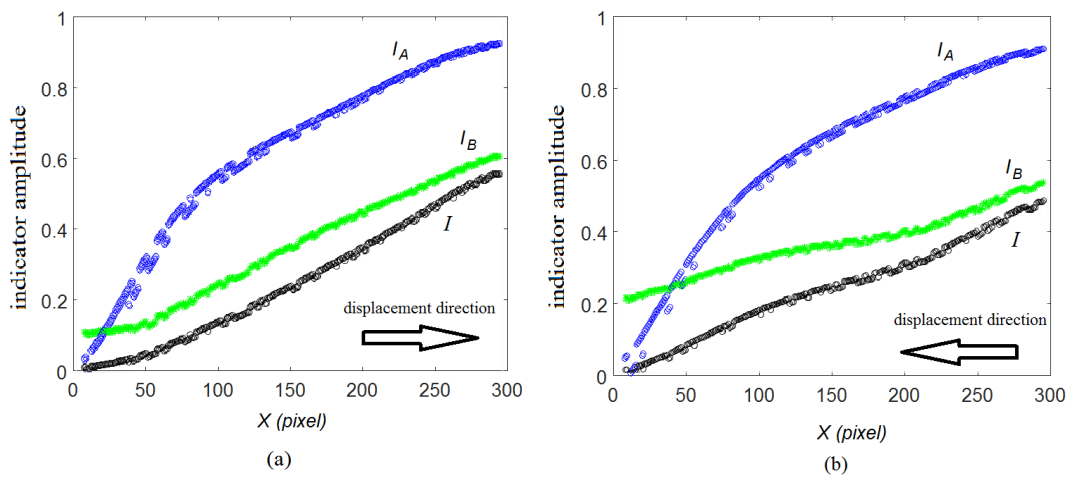


Figure 6.  $I_A$ ,  $I_B$  and  $I = I_A * I_B$  indicators as a function of pixel x for a non constant 0-3 mm crack depth :  $h(x) = x/100$  (mm). Thermal diffusion length at lowest speed  $\mu_{max} = 2.3$  mm. Crack shadow pixels:  $\Delta y = 4$  pixels. Displacement direction (a) increasing x (b) decreasing x.

The  $A_{sh}/A_0$  maximum value depends on the chosen lowest frequency (speed). The thermal sensitivity is better for low frequency (speed) but the synchronous acquisition process may shift near DC measurements. To take into account the spatial dependency of the chosen experimental parameters (maximum thermal length  $\mu_{max}$  and distance  $d$ ) the depth evaluation is calculated with the following proposed equation:

$$h_{ev} = I * (\mu_{max} * d)^{0.5} * h_{max} \quad (3)$$

where  $h_{max}$  is the maximum depth sensitivity, around 3 mm and  $I=I_A*I_B$ . The distance  $d$  should be chosen around the minimum value of  $\mu$ , that is to say the diffusion length at highest frequency (speed).

Different simulations with varying spatial parameters are presented in Figure 7. The scanning is operated in the two directions (increasing and decreasing  $x$ ) and the obtained depths for the two directions are averaged. Figure 7a shows the depth evaluation obtained using (3) for a constant  $d = 1 \text{ mm}$  and a non constant distance  $d$  (with 30% of variation). It can be seen that the calculated depth is little dependant on  $d$  if the  $\mu$  domain variation is correctly chosen. In Figure 7b, the depth evaluations obtained for 40  $\mu\text{m}$  and 80  $\mu\text{m}$  crack width are compared. The obtained depths  $h_{ev}$  have almost the same profile as for the simulation, regardless of the crack width. Consequently, the method allows thus to evaluate the crack depth with poor dependency on the crack width.

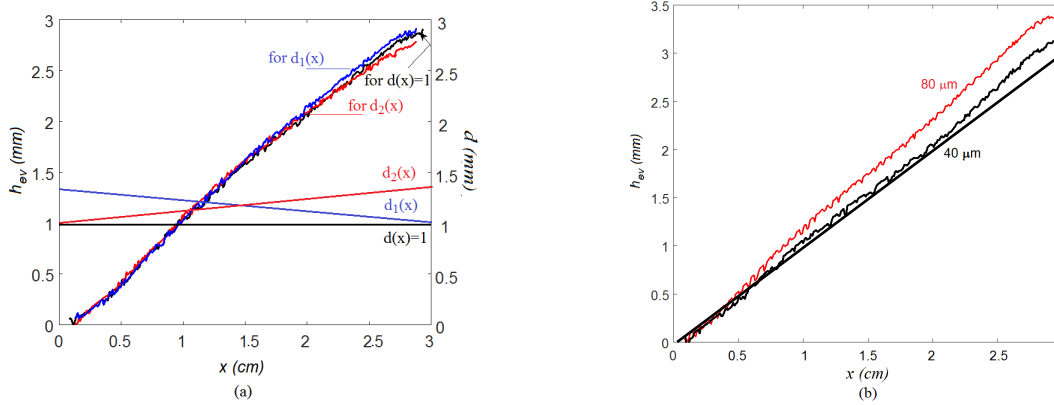


Figure 7. Depth evaluation  $h_{ev}$  in mm as a function of position  $x$  in cm for a non-constant 0-3 mm crack depth ( $h(x) = x/10$ ). Figure 7a for different  $d(x)$  shapes in mm and  $40 \mu\text{m}$  width. Figure 7b for 2 simulated widths and constant distance ( $d = 1$  mm). The line corresponds to the expected depth.

## 5. Experimental results and analyses

The experimental set up includes a heat source (diode pumped Ytterbium laser at 800 nm wavelength) and an infrared camera including a 240x320 pixel array of InSb detectors sensitive in the 3-5  $\mu\text{m}$  wavelength range. The frame rate is 100 Hz and the spatial resolution is around  $100 \mu\text{m}$ . The laser source has a 2W circular spot of 0.5 mm diameter.

Two  $40 \times 40 \times 20 \text{ mm}^3$  steel alloy plates separated by  $40 \mu\text{m}$  thick brass sheet are assembled with screws to simulate a sample with a vertical open crack. The brass is obliquely cut in  $z$  direction so as to leave an air gap to obtain an artificial non uniform (0-4mm) crack depth. Brass, with its good thermal conductivity, is used instead of steel to compensate partially the thermal contact on both plates. Experimental tests are carried out to access to the depth evaluation on this artificial non uniform crack in the steel alloy plate, using the multi-frequency and the multi-speed laser lock-in thermography methods. The measured thermal diffusivity of the plate [13] is equal to  $4.5 \pm 0.3 \cdot 10^{-6} \text{ m}^2 \text{ s}^{-1}$  and the crack distance  $d$  is around 2mm.

The images of Figure 8 show the amplitude images obtained using a static heating spot at 2 frequencies (Figure 8a and 8b) and using a moving spot at 2 speeds (Figure 8c and 8d). The heat diffusion is clearly blocked by the crack for the lower frequency in Figure 8b (compared to Figure 8a) and for the lower speed in Figure 8d (compared to Figure 8c). The amplitude temperature variations depend on the surface emissivity of the sample and are typically around a few degree.

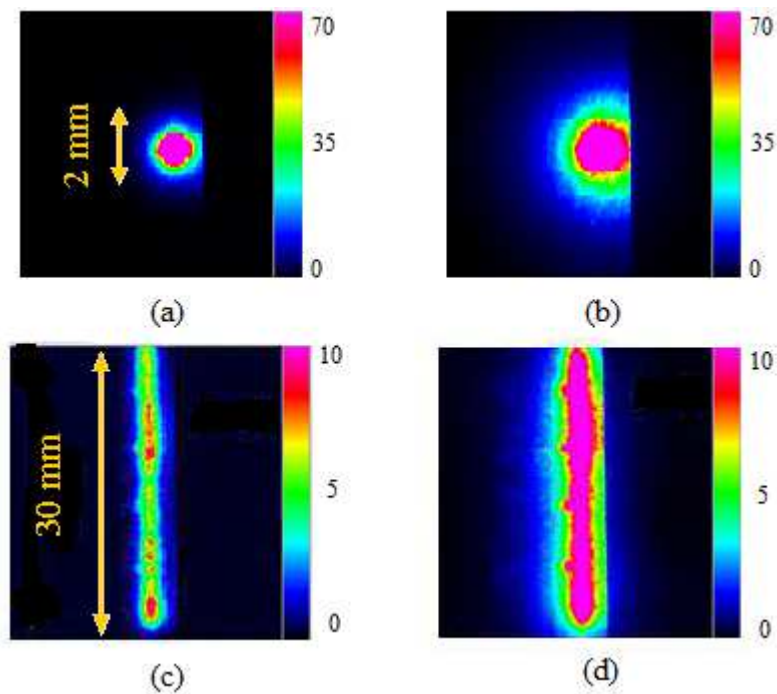


Figure 8. IR amplitude images (arbitrary units a.u.) obtained on steel alloy sample using the multi-frequency laser lock-in thermography method (a)  $f = 1$  Hz (b)  $f = 0.1$  Hz and the multi-speed laser lock-in thermography method (c)  $\Delta t = 0.5$  s (d)  $\Delta t = 5$  s. The crack is on the right of the heating source.

Using the multi-frequency laser lock-in method, the experimental results are obtained from the IR images of 5 amplitude modulation frequencies (from 1 Hz to 0.05

Hz). Using the multi-speed laser lock-in method, the experimental results are obtained from the IR images of 5 laser displacement speeds ( $L = 3$  cm scanned within 1 s to 16 s). The post processing procedure uses Equation (3) for the two methods. The only difference is the calculation of the thermal diffusion length: for the multi-frequency laser lock-in method, (1) is taken for the thermal diffusion length  $\mu$  and for the multi-speed laser lock-in method, (2) is taken instead.

The depth is evaluated with the laser on the right of the crack (heating area on the right side, Figure 9) and with the laser on the left of the crack (heating area on the left side, Figure 10).

With a 2W continuous laser power and a high sensitivity IR camera, the multi-speed laser lock-in method allows to evaluate 3 mm crack depth on crack of 3-cm length (Figure 9a and Figure 10a). The multi-frequency laser lock-in method allows to obtain local higher temperature variation, thus a better signal to noise ratio, but the scanned area is only few millimetre wide (Figure 9b and Figure 10b).

Comparing Figure 9a and Figure 9b (respectively Figure 10a and Figure 10b), the experimental results obtained with these two experimental methods are very coherent.

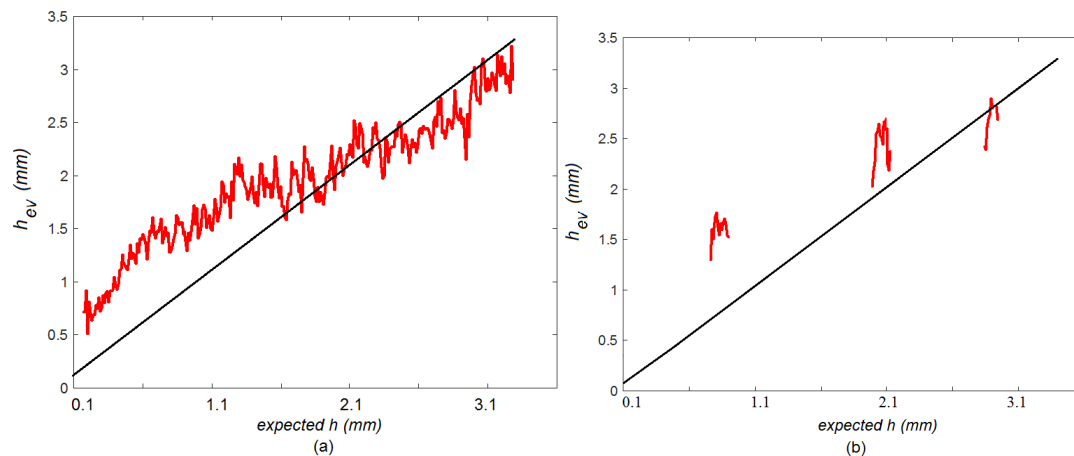


Figure 9. Depth evaluation  $h_{ev}$  in mm as a function of expected  $h$  in mm for a non constant 0-4 mm crack depth in steel allow plate (heating area and reference area on the right side of the crack). The black line corresponds to the actual depth. Laser power:  $P = 2$  W. (a) Scanning method with  $h_{ev}$  averaged for the two laser directions in x. Length along the crack:  $\Delta x = 3$ cm,  $\Delta t$  is between 0.5 s to 5 s. (b) Heating spot method at 3 positions.  $f$  is between 1 Hz to 0.05 Hz.

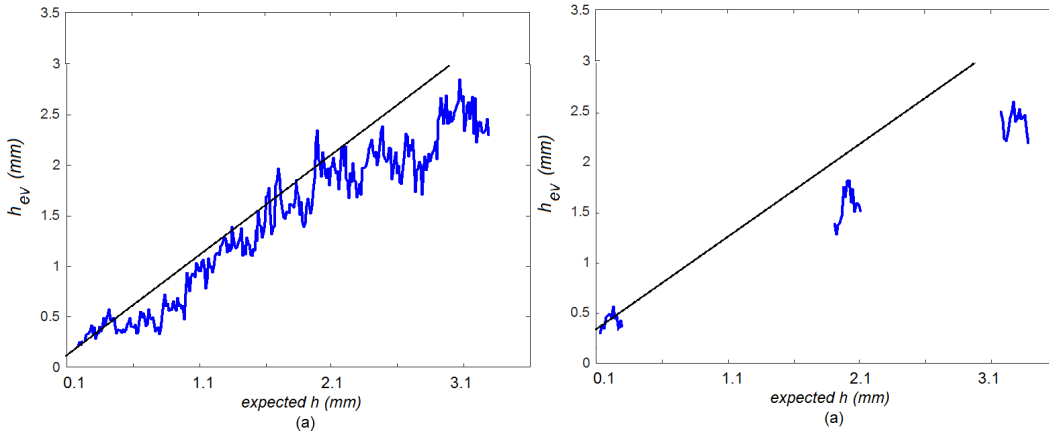


Figure 10. Depth evaluation  $h_{ev}$  in mm as a function of expected  $h$  in mm for a non constant 0-4 mm crack depth in steel allow plate (heating area and reference area on the left side of the crack). The black line corresponds to the actual depth. Laser power:  $P = 2$  W. (a) Scanning method with  $h_{ev}$  averaged for the two laser directions in x. Length along the crack:  $\Delta x = 3$ cm,  $\Delta t$  is between 0.5 s to 5 s. (b) Heating spot method at 3 positions.  $f$  is between 1 Hz to 0.05 Hz.

The differences between Figure 9 and Figure 10 are principally due to the non uniform emissivity of the surface sample which induces a bias in the normalization process. To reduce the bias on non uniform surface emissivity, can be averaged the results obtained for one side (right or left) in a direction with the result obtained for the other side (left or right) for the opposite directions as shows in Figure 11. The two obtained stackable curves give a coherent depth evaluation. The obtained values are representative to the expected depth up to 2 mm depth with about 10% uncertainty.

Above 2 mm, the curves show a less good sensitivity. The use of larger laser intensity and still lower frequency could compensate for this effect.

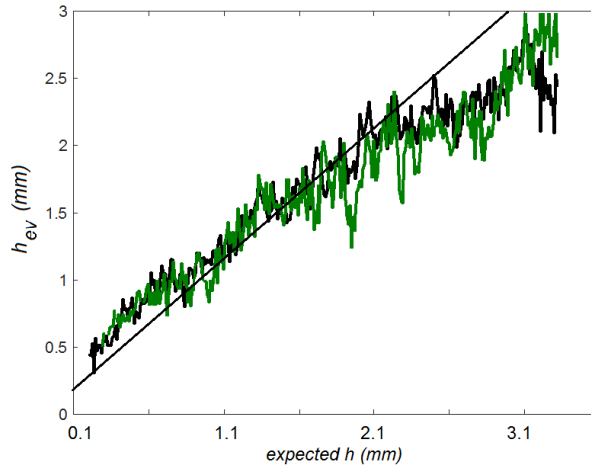


Figure 11. Depth evaluation  $h_{ev}$  in mm as a function of expected depth in mm for a non constant 0-4 mm crack depth in steel allow plate. The depth profiles (black and green curves) are obtained by averaging the results of one side with  $x$  increasing and other side with  $x$  decreasing. The line corresponds to the actual depth. Experimental conditions: Length along the crack:  $\Delta x = 3$  cm; laser power:  $P = 2$  W;  $\Delta t$  is between 0.5 s to 5 s.

In these experiments, the total camera acquisition duration is around 1 min for 5 multi-frequencies lock-in method with 2 period averaging. The total camera acquisition duration is around 2 min for 5 multi-speeds lock-in method with 2 period averaging and 2 scans. Table 1 resumes the major experimental results of the two methods.

Table 1. Major experimental results for the 2 presented methods

Method	<i>Multi-frequency</i>	<i>Multi-speed</i>
Crack depth sensitivity with a 2W laser power	[0.3-3.3 mm]	
Camera acquisition	30 s	

duration for 5 frequencies or speeds (no average)		
Camera acquisition duration for 5 frequencies or speeds (with average)	1 min	2 min
Scanned crack length	<b>Few mm</b>	<b>Few cm</b>

## 6. Conclusion

The multi-frequency lock-in IR thermography method and the multi-speed lock-in IR thermography method are two experimental methods which allow to evaluate crack depth, independently of their width. However, the sharp edges of the crack could induce not controlled IR emissions and thus uncertainties in crack depth estimation.

New indicators located in the shadow of the crack (not on the crack) are proposed. The normalized evolution of these indicators is analysed by simulations for different distance between crack and heating spot positions and for two crack widths (40  $\mu\text{m}$  and 80  $\mu\text{m}$ ). The simulations show that these indicators are not much impacted by distance variations and are a little width dependent. Measurements with an IR camera obtained with a controlled “crack” in steel blocks validate the new development: the experimental results are improved.

The multi-frequency lock-in IR thermography method evaluates cracks of a few millimetres long. This method is indicated for the investigation of complex geometries where the displacement of a laser beam onto the surface is not easy. The multi-speed continuous heating source associated with a lock-in detection allows to evaluate cracks of a few centimetre long. No surface preparation and no calibration procedure are

necessary. These depth evaluation methods are non-polluting, non-destructive and with simple optical adjustments.

#### REFERENCES

1. Balageas, D., X. Maldague, D. Burleigh, V. P. Vavilov, B. Oswald-Tranta, J.-M. Roche, C. Pradere, et G. M. Carlomagno. « Thermal (IR) and Other NDT Techniques for Improved Material Inspection ». *Journal of Nondestructive Evaluation* 35, no 1 (1 mars 2016): 18. <https://doi.org/10.1007/s10921-015-0331-7>.
2. Ciampa, F., Mahmoodi, P., Pinto, F. & Meo, M. Recent Advances in Active Infrared Thermography for Non-Destructive Testing of Aerospace Components. *Sensors* 18, 609 (2018).
3. Mohan, A. & Poobal, S. Crack detection using image processing: A critical review and analysis. *Alexandria Engineering Journal* (2017). doi:10.1016/j.aej.2017.01.020
4. Thiam, A., Kneip, J-C., Cicala, E., Caulier, Y., Jouvard, J-M., et Mattei, S., « modeling and optimization of open crack detection by flying spot thermography », *NDT&E International*, 89, 67-73, (2017).
5. Schlichting, J., Maierhofer, C. & Kreutzbruck, M. Crack sizing by laser excited thermography. *NDT and E International*, 45, n°1, 133–140 (2012).
6. Myrach, P., Ziegler, M., Maierhofer, C. & Kreutzbruck, M. Influence of the acquisition parameters on the performance of laser-thermography for crack detection in metallic components. *AIP Conference Proceedings* 1581, 1624–1630 (2014).
7. Qiu, J., Pei, C., Liu, H. & Chen, Z. Quantitative evaluation of surface crack depth with laser spot thermography. *International Journal of Fatigue* 101, 80–85 (2017).
8. Celorrio R., Omella A. J., Mendioroz A., Oleaga A., ·Salazar A., Advances in Crack Characterization by Lock-In Infrared Thermography, *Int J Thermophys* (2015) 36:1202–1207, DOI 10.1007/s10765-014-1676-3
9. Rodríguez-Martín, M., Lagüela, S., González-Aguilera, D. & Martínez, J. Prediction of depth model for cracks in steel using infrared thermography. *Infrared Physics & Technology* 71, 492–500 (2015).

10. Beuve S., Qin Z., Roger J.-P., Holé S., and Boué C. Open cracks depth sizing by multi-frequency laser stimulated lock-in thermography combined with image processing. *Sensors and Actuators A: Physical*, 2016
11. Boué C. and Holé S., Open crack depth sizing by multi-speed continuous laser stimulated lock-in thermography  
*Meas. Sci. Technol.* 28, 065901, 2017
12. Y. Fedala, M. Streza, F. Sepulveda, J.-P. Roger, G. Tessier, C. Boué, Infrared lock-in thermography crack localization on metallic surfaces for industrial diagnosis, *Journal of Non Destructive Evaluation*, DOI 10.1007/s10921-013-0218-4, 2013
13. C. Boué , S. Holé, Infrared thermography protocol for simple measurements of thermal diffusivity and conductivity, *Infrared Phys. Tech.* 55 376-79, 2012